



# INTERNATIONAL JOURNAL OF MEDICAL

ARTS

Volume 7, Issue 8 (August 2025)



http://ijma.journals.ekb.eg/

P-ISSN: 2636-4174

E-ISSN: 2682-3780



### Available online at Journal Website https://ijma.journals.ekb.eg/ Main Subject [Radiology]



### **Original Article**

### Comparison between Whole Body Diffusion MRI and FDG PET/CT in Detection of Metastatic Disease

Mohamed Shawky Alwarraky\*; Mohamed Mohamed Houseni; Hazem Metwaly Omer; Heba El-Desouky Fath-Allah

Department of Diagnostic and Interventional Medical Imaging, National liver institute, Menoufia University, Shebin Elkom, Menoufia, Egypt.

### **Abstract**

**Article information** 

**Received:** 08-05-2025 **Accepted** 18-06-2025

DOI: 10.21608/ijma.2025.383258.2182

\*Corresponding author

Email: hebaeldesouky380@ gmail.com

Citation: Alwarraky MS, Houseni MM, Omer HM, Fath-Allah HE. Comparison between Whole Body Diffusion MRI and FDG PET/CT in Detection of Metastatic Disease. IJMA 2025 August; 7 [8]: 5977-5991. doi: 1021608/ijma.2025.383258.2182.

Background: Technological advancements and continual enhancements in imaging modalities have significantly increased the sensitivity of cancer detection and diagnosis. Among these, 18F-fluorodeoxyglucose positron emission tomography/computed tomography [\*F-FDG PET/CT] is widely regarded as the reference standard for staging the majority of malignancies and evaluating disease distribution, as it provides both functional and anatomical data within a single whole-body examination. In clinical settings where PET/CT is unavailable, conventional cross-sectional imaging techniques such as CT and MRI are typically employed for staging purposes.

The aim of the work: This study aimed to evaluate and compare the diagnostic performance of whole-body diffusion-weighted MRI [WB-DWI] and <sup>18</sup>F-FDG PET/CT in detecting metastatic disease in cases with various primary malignancies.

Patients and Methods: A prospective research with 30 cases [aged 18–74 years] with confirmed metastatic lesions originating from different primary tumors underwent WB-DWI within one week of undergoing <sup>18</sup>F-FDG PET/CT, to ensure temporal consistency of imaging data. A consultant radiologist interpreted the MRI findings. For both PET/CT and WB-DWI, diagnostic performance metrics; including overall agreement, sensitivity, specificity, and positive and negative predictive values [NPV] were calculated.

Results: The findings demonstrated strong concordance between WB-DWI and <sup>18</sup>F-FDG PET/CT in the detection of hepatic, osseous, peritoneal, and adrenal metastases. Moderate agreement was observed in the identification of pulmonary, lymph nodal, and cerebral metastases. Across all metastatic sites, the mean ADC values were significantly lower than those of corresponding healthy tissues

Conclusion: WB-DWI presents as a viable imaging alternative for the detection of visceral and skeletal metastases in cases with solid tumors, demonstrating diagnostic accuracy similar to that of <sup>18</sup>F-FDG PET/CT. Metastatic lesions consistently exhibit reduced ADC values relative to normal tissues. While WB-DWI shows moderate to good agreement with PET/CT for metastasis detection, the combined application of both modalities enhances diagnostic accuracy and increases the likelihood of identifying additional metastatic sites.

Keywords: 18F-FDG PET/CT; Hepatocellular Carcinoma; WB-DWMRI; Subtraction MRI; DWI-HCC Response.



This is an open-access article registered under the Creative Commons, ShareAlike 4.0 International license [CC BY-SA 4.0] [https://creativecommons.org/licenses/by-sa/4.0/legalcode.

### INTRODUCTION

Cancer remains a potentially curable condition, with substantial declines in mortality over the past two decades attributed primarily to advances in early detection and the implementation of adjuvant systemic therapies <sup>[1]</sup>. Metastatic lesions are frequent presentations in advanced malignancies and are increasingly encountered in routine clinical practice, raising important diagnostic and therapeutic considerations <sup>[2]</sup>. The diagnostic assessment of oncologic cases typically involves staging procedures that are integral to therapeutic decision-making and prognostication <sup>[3]</sup>.

Conventional cross-sectional imaging modalities, including computed tomography [CT] and magnetic resonance imaging [MRI], have long served as standard techniques for the detection of metastatic disease, offering acceptable levels of sensitivity and specificity [4]. The integration of positron emission tomography with CT [PET/CT], particularly when employing the radiotracer 18F-fluoro-2-deoxyglucose [18F-FDG], has demonstrated considerable utility as a problem-solving modality in cases of cancer of unknown primary origin [5].

PET/CT facilitates whole-body imaging and enables assessment of tumor metabolic activity, supporting its role in both initial staging and treatment response evaluation. Nevertheless, its diagnostic performance may be constrained by factors such as physiologic uptake in nonpathological tissues, inter-lesional variability in tracer accumulation, elevated radiation exposure, and limited resolution for lesions smaller than 1 cm [6]. Given these limitations, there is a critical need for imaging modalities that enable comprehensive tumor evaluation, enhance lesion characterization, and improve monitoring of therapeutic response, all while minimizing radiation exposure. In this context, advancements in whole-body MRI [WB-MRI] have facilitated full-body anatomical imaging using T1- or T2-weighted sequences at 1.5 Tesla [T] field strength [7]. Diffusion-weighted MRI [DW-MRI], a quantitative MR technique, assesses the Brownian motion of water molecules within tissues and offers additional insight into tumor microstructure [8]. Advanced quantitative MRI parameters such as diffusion-weighted imaging [DWI] with Apparent Diffusion Coefficient [ADC] maps, and dynamic contrast-enhanced [DCE]-MRI can provide metrics of the molecular and vascular characteristics of tumors [9].

### THE AIM OF THE WORK

This work compared between whole-body diffusion MRI [WB-DW-MRI] and FDG PET/CT in detection of metastatic disease in cases with different primary malignancies.

### PATIENTS AND METHODS

This prospective research was conducted on 30 cases with metastases from different primary malignancies at the diagnostic medical imaging and interventional radiology department at National Liver Institute Hospitals; Menoufia University between December 2022 to January 2025. There was no age or gender predilection. We included cases with histo-pathologically diagnosed primary malignant tumors and underwent US, CT, PET/CT, or MRI to screen for suspected metastasis, cases for metastatic workup, and cases who agreed to do WB-DWI. However, we excluded from the research: Cases with no histopathologically proved malignancy, lactating and pregnant females, uncontrolled diabetes or elevated blood sugar more than 200 mg/dl, cases refusing to do WB-DWI, and cases with contraindications to MRI [such as claustrophobia and implanted pacemakers].

All eligible cases signed an informed consent after full explanation of the research aim, producers and assurance of all case rights. In addition, the research protocol was reviewed and approved by medical research and the National Liver Institute Ethics Committee [REC] [N-00373-2022] [Menoufia University]. All included cases subjected to a consent taking, clinical assessment, checking for contraindication to MRI imaging [such as claustrophobia and implanted pacemakers], laboratory investigations including complete blood count, fasting blood sugar, and tumor markers, and radiological investigations [both wholebody DWI and <sup>18</sup>F-FDG PET/CT within an average of 3 days [range, 0-7 days] of each other to ensure stationary data. They were followed up for 6 months, both clinically and by imaging [CT, PET/CT, or MRI]].

To minimize interpretive bias, the radiologists interpreting the WB-DWI and PET/CT images were blinded to each other's findings. This approach ensured independent assessment of each imaging modality.

Case Preparation and Radiopharmaceutical Administration:

Prior to the imaging procedure, each case underwent the placement of an intravenous cannula to facilitate the administration of the radiopharmaceutical agent. The administered agent was <sup>18</sup>F-FDG, a glucose analog used in nuclear medicine imaging, which was injected at a calculated dosage of 0.1 millicurie per kilogram of body weight. After receiving the radiotracer, the case was made to rest comfortably in a specially designated uptake room with minimal sensory stimulation. This room was dimly lit and quiet to ensure the case remained relaxed, which is critical for reducing non-specific muscular uptake of the

radiotracer. The case was covered with warm blankets to maintain body temperature, as hypothermia can alter tracer biodistribution. During the 60 to 70 minute uptake period, the case was advised to refrain from engaging in activities that may increase muscular uptake of <sup>18</sup>F-FDG, such as speaking, reading, or chewing. Immediately before the scan commenced, the case was instructed to void the urinary bladder to lower background activity in the pelvic region.

PET/CT Image Acquisition: The imaging study was carried out using an advanced integrated PET/CT scanner equipped with a 128-slice multi-detector computed tomography [CT] component. Initially, a lowdose CT scan was acquired for anatomical localization and attenuation correction, covering the region from the base of the skull to the upper thigh. This step was essential for accurate co-registration of functional and anatomical data. Following the CT acquisition, three-dimensional mode positron emission tomography [PET] data were acquired. Each bed position was scanned for three minutes to ensure adequate photon collection and image quality. Image reconstruction was performed using iterative reconstruction algorithms known to enhance image quality and lesion detectability. The specific method utilized was a combination of True X and time-of-flight [TOF] reconstruction, which included two iterations and twenty-one subsets. The axial field of view for each bed position was set to 11.4 centimeters. Reconstruction also employed a Gaussian filter with a full-width at half-maximum [FWHM] value of 4.0 millimeters, and scatter correction was applied to reduce noise and enhance contrast.

**Diagnostic CT Scanning Protocol:** For cases requiring additional anatomical assessment, a diagnostic CT scan was acquired following PET imaging. This scan used a set of standardized parameters: 350 milliamperes tube current, 120 kilovolts tube voltage, 0.5-second gantry rotation time, 5-millimeter slice thickness, 8-millimeter table feed, and a 2.5-millimeter reconstruction increment. This non-contrast-enhanced diagnostic CT was performed in cases with contraindications to iodinated contrast agents, such as elevated serum creatinine levels exceeding 2.0 mg/dL or a known history of allergic reactions to contrast

media. In cases where contrast enhancement was clinically warranted, cases received intravenous administration of iodinated contrast medium [Optray 300] at a dosage of 1.5 to 2 milliliters per kilogram of body weight. The contrast agent was delivered using a power injector at a rate of 4 milliliters per second. Imaging was carried out in multiple phases, including arterial phase at 20 seconds post-injection, portovenous phase at 60 seconds, and delayed phase at 300 seconds. The scan range was consistent with that used for low-dose CT and PET imaging. A breath-hold technique was used during CT acquisition to minimize motion artifacts and optimize image quality.

Image Review and Analysis: PET images corrected for attenuation, low-dose CT images, and contrast-enhanced CT images were automatically fused using specialized imaging software. These fused images were transferred to advanced image analysis workstations for further interpretation. Either lesions identified as primary tumors or metastases were evaluated across multiple organ systems, including but not limited to the lymph nodes, liver, lungs, bones, peritoneum, and adrenal glands.

Evaluation of FDG-PET Images: The PET images were analyzed in multiple orthogonal planes—axial, sagittal, and coronal—to ensure comprehensive visualization of tracer distribution. Areas showing increased <sup>18</sup>F-FDG uptake were interpreted as sites of potential disease activity. Hepatic lesions were deemed suspicious if tracer uptake exceeded that of surrounding liver parenchyma. Pulmonary metastases were identified by any detectable FDG uptake, irrespective of their absolute intensity. Hypermetabolic activity in lymph nodes, bone, or adrenal glands—greater than that of the blood pool—was considered indicative of metastatic disease. A semi-quantitative assessment was also performed using the standardized uptake value [SUV max], measured by placing a circular region of interest over the most metabolically active portion of each lesion.

**Evaluation of CECT Images:** The contrast-enhanced CT images were interpreted in axial, coronal, and sagittal planes. Bone lesions were assessed using the bone window setting, while lung lesions were reviewed using the lung window to ensure optimal visualization. Criteria for metastatic disease included lymph nodes with a short axis diameter exceeding 1-centimeter, hepatic lesions demonstrating focal enhancement, pulmonary nodules larger than or equal to 8 millimeters, lytic lesions within the bone marrow, and enhancing soft tissue abnormalities.

Fused PET-CT Image Interpretation: Lesions identified separately on PET and CT were re-examined on the fused images to confirm the anatomical correlate of functional abnormalities. Lesions were classified as metastatic if they showed FDG uptake exceeding the blood pool and/or contrast enhancement on CT. For example, lymph nodes larger than 1 centimeter that also showed hypermetabolism were flagged as positive. Similarly, liver lesions demonstrating increased FDG uptake or contrast enhancement, pulmonary nodules with FDG uptake, and bone lesions with both lytic changes and FDG activity were considered metastatic. If contrast-enhanced imaging was indicated, a contrast CT was performed after intravenous administration of 1.5-2 ml/kg of iodinated contrast [Optray 300], using an automated injector [Medrad Stellant] at a flow rate of 4 ml/s. The arterial phase was acquired 20 seconds post-contrast injection, followed by the portovenous phase at 60 seconds and the delayed phase at 300 seconds. The scanning range for contrast-enhanced CT was identical to that used in the low-dose and PET scans [from the skull base to the upper thighs]. A limited breath-hold technique was employed to minimize motion artifacts during the imaging process. All data were acquired using a

combined PET/CT system, which integrates a PET scanner with a multislice helical CT scanner, allowing for the acquisition of co-registered CT and PET images within a single session.

### Whole-Body Diffusion-Weighted Imaging [DWI] MRI Protocol

Case Preparation: Cases scheduled for whole-body MRI underwent standard preparation procedures, including changing into gowns free of any metallic components and removing all personal items that could interfere with the magnetic field. No intravenous contrast agent was administered during the MRI examination, as the sequences used provided sufficient diagnostic information without the need for contrast enhancement.

Imaging Technique and Sequence Parameters: Imaging was conducted using a high-field 1.5 Tesla GE 450w MRI scanner equipped with a Q-body coil to enable whole-body coverage. Cases were placed on an extended anatomical table that utilized rolling-table technology to facilitate continuous imaging from head to thigh. The examination protocol included several pulse sequences. These included T1-weighted Turbo Spin Echo [TSE], T2-weighted Short Tau Inversion Recovery [STIR], and Diffusion-Weighted Imaging with Background Suppression [DWIBS] using a single-shot echo-planar imaging technique. These sequences were performed in free-breathing mode to ensure case comfort and to enable acquisition over a larger anatomical range.

**T1-Weighted Imaging:** The T1-weighted TSE sequence was acquired in the coronal plane with a slice thickness of 6 millimeters and an inter-slice gap of 1 millimeter. A total of 39 slices per station were obtained, with a field of view set to 530 by 265 millimeters. The acquisition matrix was 208 by 287, reconstructed to 512. The voxel dimensions were 1.27 by 1.85 by 6.00 millimeters. The total scan time for this sequence was 63 seconds.

**STIR Imaging:** The STIR sequence was also acquired in the coronal orientation and mirrored the parameters of the T1-weighted sequence. Slice thickness and inter-slice gap were maintained at 6 and 1 millimeters, respectively, with the same number of slices per station. The acquisition matrix was set at 336 by 121, with reconstruction to 512. Voxel size was 1.58 by 2.18 by 6.00 millimeters. Two acquisitions were performed per sequence, with each taking approximately 62 seconds.

**DWIBS Imaging:** The DWIBS sequence utilized single-shot EPI and was performed in the axial plane. The parameters included a slice thickness of 6 millimeters with no inter-slice gap. Each station captured 44 slices, with a field of view measuring 530 by 303 millimeters. The acquisition matrix was 108 by 61, reconstructed to 352. The voxel size was 4.91 by 4.83 by 6.00 millimeters. Two diffusion b-values—50 and 800 s/mm²—were used to optimize lesion detection. The half-scan factor was 0.627, and each sequence required approximately 3 minutes and 29 seconds to acquire.

Total Imaging Duration and Reconstruction: The entire examination took approximately 25 to 30 minutes to complete. All scans were performed during free-breathing, and no intravenous contrast was used. Axial DWIBS images were reconstructed into radial and coronal planes. Radial reconstructions used 20 projections to create a volumetric dataset, while coronal reconstructions had a slice thickness of 4 millimeters with a 1-millimeter gap. Forty-four images were acquired per station. These images were then merged to produce a continuous, whole-body DWIBS image.

### MRI Image Analysis

### A. Qualitative Analysis

The qualitative evaluation of WB-MRIs involved the reconstruction and interpretation of images derived from T2WI, DWI, and ADC maps. These datasets were processed inline on an advanced medical imaging workstation, allowing for high-resolution visualization and consistent anatomical segmentation. The WB-MRI scans were divided into standardized anatomical regions, including the head, neck, thoracic cavity, abdominal cavity, pelvic region, and lower extremities, to ensure comprehensive assessment of the entire body.

Within each anatomical segment, radiologists carefully inspected the images to identify and enumerate any suspicious lesions. The interpretation was based on signal intensity characteristics observed across different sequences. Lesions classified as benign typically presented with low signal intensity [hypointensity] on DWI sequences and high signal intensity on corresponding ADC maps. These signal characteristics are indicative of free water diffusion, commonly seen in non-malignant tissue. On the other hand, malignant lesions frequently exhibited restricted diffusion, appearing as hyperintense [bright] areas on DWI and demonstrating reduced signal intensity [hypointensity] on ADC maps. These features are consistent with densely packed cellular structures, which limit the movement of water molecules.

It is noteworthy that certain regions with markedly reduced signal on both DWI and ADC sequences were interpreted as areas of necrosis or non-viable tissue. Such necrotic components were excluded from further analysis, as they do not reliably contribute to the characterization of lesion viability or malignancy.

### **B.** Quantitative Analysis

The quantitative analysis of DWI focused on generating and analyzing ADC maps for both normal and abnormal tissue regions. Regions of interest [ROIs] were manually delineated on ADC maps by experienced radiologists. These ROIs were strategically drawn to encompass areas representative of both healthy tissue and suspected lesion tissue. For abnormal tissue evaluation, ROIs were defined using data acquired at multiple b-values [0, 500, and 800 s/mm²] to capture the full extent of diffusion properties. ADC values were then calculated for each lesion, including the mean and standard deviation, to provide a quantitative measure of diffusion restriction.

To establish baseline ADC values for normal anatomical structures, ROIs were placed over diverse organ systems including the brain, lungs, breasts, liver, peritoneum, adrenal glands, and osseous structures. For these normal tissues, large and homogenous areas were selected to ensure representative sampling. Conversely, for lesion tissue, a semi-automated region-growing technique was employed to trace the lesion boundaries accurately. This method was supplemented by morphological operations to refine the contours of the ROI and ensure that measurements remained confined within the lesion margin.

Image Interpretation: Interpretation of WB DWI images was carried out with the aim of identifying lesions that demonstrated diffusion restriction. Each case was independently reviewed to detect the presence, anatomical location, and physical dimensions of any abnormal findings. A lesion was considered metastatic if it exhibited increased signal intensity on DWI at a high b-value [specifically b = 800 s/mm²], which is indicative of restricted water diffusion often seen in malignant processes. Importantly, the assessment of DWI images was performed

in a blinded manner, with the reviewing radiologist unaware of the corresponding PET/CT findings. This approach was intended to prevent interpretive bias. A separate dataset was compiled to document the DWI findings. Similarly, PET/CT imaging was evaluated independently in a different reading session, also blinded to the DWI results. All relevant lesion characteristics—such as anatomical site, lesion size, and classification as benign or malignant—were meticulously documented in a dedicated data file. Following the completion of these independent analyses, all datasets were merged for integrated review. In instances where ambiguity persisted or confirmation was necessary, additional conventional imaging modalities [such as ultrasound, CT, or targeted MRI] were utilized to support diagnostic decision-making.

Reference Standard for the Definition of a Positive Lesion: A consensus-based reference standard was employed to determine the final classification of each lesion as either positive [metastatic] or negative [benign]. This consensus assessment was performed in a separate session at the end of a 6-month follow-up period, during which all relevant patient data—clinical, laboratory, histopathology, or nuclear scintigraphy studies—were gathered, as requested by the attending physicians.

A lesion detected by PET/CT imaging was classified as metastatic if any one of the following criteria was satisfied:

- 1. The lesion, or at least one lesion in a cluster of multiple lesions, was confirmed by histopathological analysis.
- The lesion displayed an imaging pattern consistent with metastatic disease, and was associated with either: a measurable increase in size during follow-up imaging, or the appearance of a new lesion with similar imaging characteristics as the initial lesion, irrespective of whethe r treatment was administered.

Lesions were classified as definitively benign only if the imaging pattern was typical of a benign lesion, and there was no increase in size or development of new lesions during follow-up imaging conducted over the 6-month period. Stability in lesion size, without any new lesion development, was considered evidence against malignancy [10].

Statistical Analysis: Statistical data analysis was performed using R Software version 4.1.2 [R Foundation for Statistical Computing, Vienna, Austria]. Categorical variables were expressed as frequencies and percentages, while continuous variables were presented as Mean ± SD with the corresponding range. To compare the ADC values between metastatic and normal tissue, a paired t-test was used. The sensitivity, specificity, positive predictive value [PPV], negative predictive value [NPV], and accuracy of whole-body diffusion MRI, PET/CT, and conventional imaging were calculated on a per-lesion basis. Receiver operating characteristic [ROC] curves were generated to assess the ability of each imaging modality to detect metastases, using histopathology and follow-up as the reference standard for all lesions. The agreement between the imaging modalities was quantified using Cohen's Kappa  $[\kappa]$ , classified as slight  $[\kappa < 0.21]$ , fair  $[\kappa = 0.21 - 0.40]$ , moderate  $[\kappa = 0.41 - 0.60]$ , substantial  $[\kappa = 0.61 - 0.80]$ , and almost perfect [ $\kappa = 0.81$  to <1.00]. Statistical significance was considered for pvalues less than 0.05. The correlation between ADC values and SUV max of metastatic lesions was assessed using the Spearman correlation coefficient [r], classified as perfect positive correlation [+1.0], strong positive correlation [+0.7 to +0.9], moderate positive correlation [+0.4 to +0.6], strong negative correlation [-0.7 to -0.9], and perfect negative correlation [-1.0].

Sample size calculation: The sample size for this study was determined using G\*Power 3.1.9.2 [Universtat Kiel, Germany]. According to **Barchetti** *et al.* [11], the sensitivity, specificity, and accuracy of Whole-body diffusion-weighted MRI [WB-DWI] were reported as 98.2%, 99.9%, and 99.3%, respectively. Additionally, the prevalence of metastasis in patients with primary tumors, as detected by 18F-FDG PET/CT [the gold standard], is approximately 90%. Using the following parameters: expected sensitivity of 98.2%, expected specificity of 99.9%, disease prevalence of 90%, acceptable precision [W] of 5%, and a significance level [ $\alpha$ ] of 0.05, the sample size for sensitivity was calculated to be 31, and for specificity, it was 16. The final required sample size, accounting for a 10% drop-out rate, is 35 participants.

### **RESULTS**

This research included 30 cases with metastases from different primary malignancies. Their age ranged from 18 to 74 years, with a mean [ $\pm$  SD] of 52.87  $\pm$  17.07 years. The metastatic lesions were classified into seven regions for simplifying analysis: liver, lung, skeletal system, lymph nodes, peritoneal, brain, and adrenals metastasis. Using combined radiological and histo-pathologically proven data as well as a follow up about 6 months as a reference standard, for each site F-18 FDG PET/CT and MRI-DWIBS results were correlated to the reference standard. Regarding liver metastasis from the 30 cases, 11 cases were detected by PET/CT, and 13 cases were detected by WB-DWIs. While PET/CT was superior to WB-DWIs for pulmonary, lymph nodal, and peritoneal metastasis, for pulmonary metastasis, WB-DWIs detected only 7 cases from 13 cases, and for lymph nodal metastasis, WB-DWI detected only 17 cases from 23 cases, and 3 cases by WB-DWIS from 4 cases by PET/CT. Regarding skeletal and brain deposits, WB-DWIs were superior to PET/CT, for skeletal metastasis PET/CT detected 14 cases from 15 cases were detected by WB-DWIs, and for brain metastasis PET/CT detected only 3 cases from 5 cases were detected by WB-DWI. [Table 1].

Out of the 30 cases were confirmed to have liver metastasis by histopathology and follow up. All the 13 cases were successfully detected by MRI-DWIBS. On the other hand, PET-CT diagnosed 11 out of these 13 cases with 2 false negative instances. Accordingly, the aforementioned data emphasize the significantly higher MRI-DWIBS sensitivity, NPV, and accuracy [P value 0.0012] compared to PET-CT [100% accuracy versus 93.3%], while the similar yield of specificity, PPV was noticed by both techniques [100%] [Table 2].

There was significantly higher MRI-DWIBS sensitivity, NPV, and accuracy [P value 0.0012] compared to PET-CT [100% accuracy versus 93.3%] in detecting liver metastasis. In addition, there was significantly higher PET/CT sensitivity, NPV, and accuracy [P value 0.0012] compared to WBDWIs [100% accuracy versus 80%] in detecting pulmonary metastasis. Furthermore, there was significantly higher WBDWIs sensitivity, NPV, and accuracy compared to PET/CT [100% accuracy versus 96.7%] in detecting bone metastatic lesions, significantly higher PET/CT sensitivity, NPV, and accuracy compared to WBDWIs [100% accuracy versus 80%] in detecting lymph node metastatic lesions, significantly higher PET/CT sensitivity, NPV, and accuracy compared to WBDWIs [100% accuracy versus 96.7%] in detecting peritoneum metastatic lesions, significantly higher MRI-DWIBS sensitivity, NPV, and accuracy compared to PET-CT [96.7% accuracy versus 90.0%] in detecting brain metastatic lesions. However, there is a similar yield of specificity [100%], PPV was noticed by both techniques [100%]. Both PET-CT and MRI-DWIBS had successfully

detected adrenal metastasis with 100 % sensitivity, specificity, PPV, NPV and overall accuracy [Figure 1].

There was good agreement between WB-MRI and PET/CT in detecting liver metastasis [WB-MRI can detect all positive 11 cases detected by PET/CT]. There is moderate degree of agreement between WB-MRI and PET/CT in detecting pulmonary metastasis [WB-MRI can detect only 7 positive cases from 13 cases detected by PET/CT]. There is good agreement between WB-MRI and PET/CT in detecting bone metastases [WB-MRI can detect all positive 14 cases detected by PET/CT]. There is a moderate degree of agreement between WB-MRI and PET/CT in detecting lymph nodal metastases [WB-MRI can detect only 17 positive cases from 23 detected by PET/CT]. There is a good degree of agreement between WB-MRI and PET/CT in detecting peritoneal metastases [WB-MRI can detect only 3 positive cases from 4 detected by PET/CT]. There is a good degree of agreement between WB-MRI and PET/CT in detecting adrenal metastases [WB-MRI can detect all three positive cases detected by PET/CT]. There is a moderate degree of agreement between WB-MRI and PET/CT in detecting brain metastases [WB-MRI can detect two positive cases from 3 cases detected by PET/CT] [Table 3].

The mean ADC values for all organs involved in metastasis were significantly reduced when compared to the corresponding healthy organs [p < 0.001].

**Table [1]:** Number of metastatic lesions detected by various protocols per case pathology

	WB-MRI	1 0,	PET/CT	
	True +ve	True -ve	True +ve	True -ve
Liver	13	17	11	17
Pulmonary	7	17	13	17
Bone	15	15	14	15
Lymph nodes	17	7	23	7
Peritoneum	3	26	4	26
Adrenal	3	27	3	27
Brain	5	24	3	24

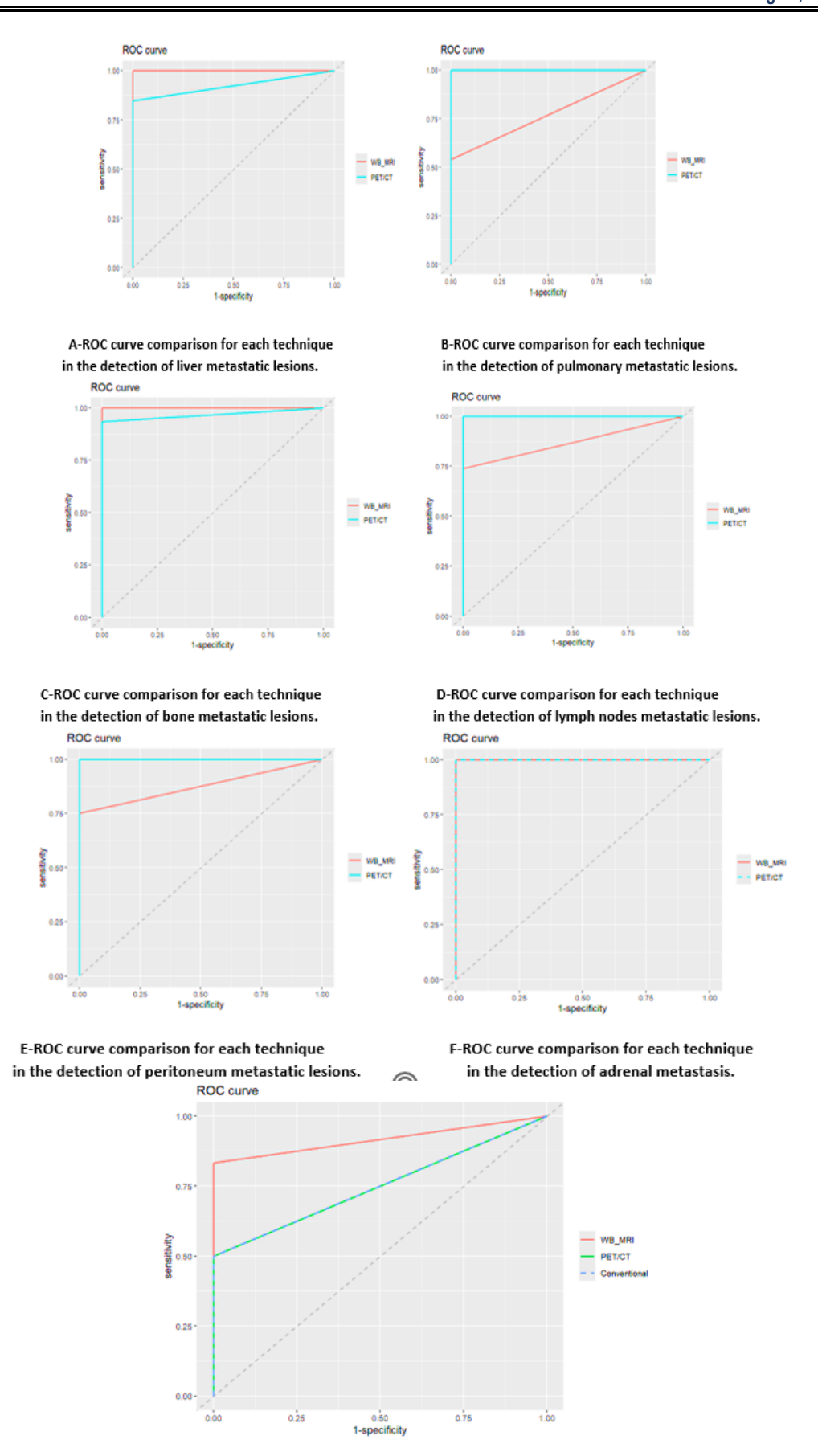
**Table [2]:** WB-MRI and PET/CT agreement in detecting metastases

		PET/CT			κ	P-Value
			+ve [n]	-ve [n]		
Liver	WB-MRI	+ve [n]	11	2	0.86	< 0.001
metastasis		-ve [n]	0	17		
Pulmonary	WB-MRI	+ve [n]	7	0	0.57	< 0.001
metastasis		-ve [n]	6	17		
Bone	WB-MRI	+ve [n]	14	1	0.93	< 0.001
metastasis		-ve [n]	0	15		
Peritoneum	WB-MRI	+ve [n]	3	0	0.84	< 0.001
metastasis		-ve [n]	1	26		
Adrenal	WB-MRI	+ve [n]	3	0	1	< 0.001
metastasis		-ve [n]	0	27		
Brain	WB-MRI	+ve [n]	2	3	0.43	< 0.001
metastasis		-ve [n]	1	24		

**Table [3]:** Comparison of ADC value between metastatic and normal tissue

	Metastatic tissue	Normal tissue	P-Value
Liver	0.72 ±0.21	$1.78 \pm 0.14$	<0.001*
Pulmonary	0.81 ±0.22	$1.76 \pm 0.18$	<0.001*
Bone	0.80 ±0.21	$1.79 \pm 0.28$	<0.001*
Lymph nodes	0.72 ±0.21	$1.85 \pm 0.26$	<0.001*
Adrenal	0.60 ±0.18	1.53 ±0.07	0.001*
Brain	$0.88 \pm 0.20$	1.77 ±0.21	<0.001*

Data are expressed as mean  $\pm$  SD. \*  $\overline{p}$  <0.05 by paired t-test.



G-ROC curve comparison for each technique in the detection of brain metastatic lesions

Figure [1]: Graph showing comparison of ROC curve for WB-MRI and PET/CT for detection of: A- Liver metastatic lesions. B- Pulmonary metastatic lesions. C- Bone metastatic lesions. D- Lymph node metastatic lesions. E- Peritoneum metastatic lesions. F-adrenal metastasis. G- Brain metastatic lesions.

### Case 1:

A 70-year-old male case was presented with left lobe hepatic focal lesion, and pulmonary nodules. She was sent for PET/CT for initial staging. Previous CT abdomen with contrast research exhibited infiltrative non enhancing focal lesion. CT chest findings exhibited multiple bilateral pulmonary nodules. PET-CT detected metabolically active bilobar hepatic focal lesions, the most active is left hepatic lobe infiltrative neoplastic lesion invading left hepatic vein and extending to IVC and right atrium with left moderate IHBRDs...HCC vs cholangiocarcinoma for histopathological assessment. Metabolically active hepatic, lymph nodal, pulmonary and osseous deposits. MRI/DWIBS detected the more number of hepatic and osseous involvement compared to PET-CT. yet, some of the pulmonary and nodal involvement were missed by DWIBS. However, the case was diagnosed as stage IV disease. Figure 2,3,4,5.

### Case 2:

A 69-year-old male case was presented with vertebral mass and multiple bone deposits and diagnosed as metastatic papillary carcinoma. Previous PET/CT exhibited metabolically active thyroid gland neoplastic lesion with metastatic pulmonary, lymph nodal and bone marrow deposits. Metabolically active right upper lung lobe neoplastic mass. Follow up staging FDG PET CT revealed metabolic and morphologic progression of thyroid gland, right upper lobe neoplastic lesions as well as metastatic pulmonary, lymph nodal and vertebral deposits. Staging WB-MRI/DWIBS detected thyroid gland, right upper lobe neoplastic lesions as well as metastatic pulmonary and lymph nodal [but less number], vertebral deposits [more lesions than PET/CT] and right adrenal deposit. Newly developed brain lesion not detected by PET/CT., all showing restricted diffusion on DWIs. So, the case was diagnosed as stage IV disease. Figure 6,7,8,9,10,11.

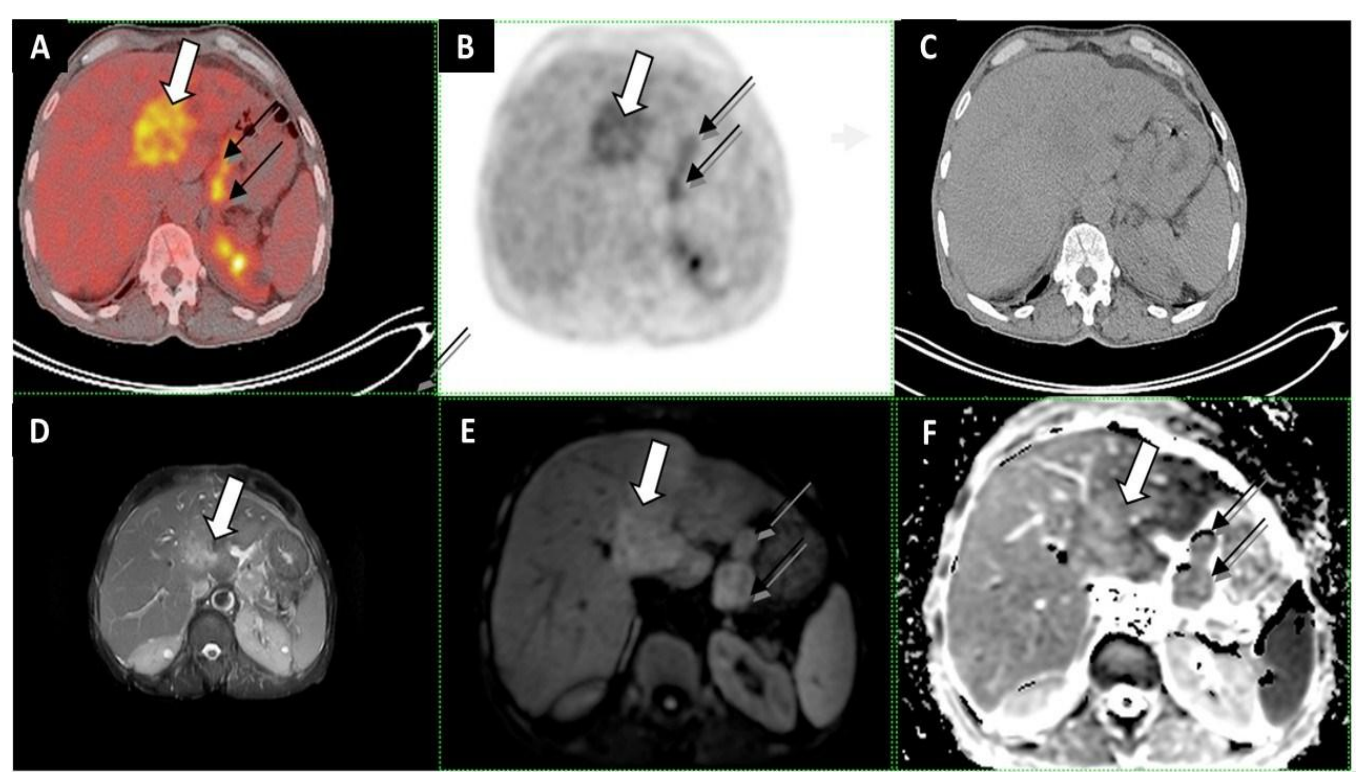


Figure [2]: Axial PET-CT versus Axial DWIBS images for the same case: a and b: Both a] axial fused PET-CT and [b] PET images demonstrating increased FDG uptake corresponding to left lobe infiltrative hypodense segments II,III,IV focal lesion with SUV max 6.2, along the course of left hepatic vein extending into IVC [white arrows], also there are enlarged left gastric and porta hepatis lymph nodes, SUV max = 5.5,[black arrows] d axial T2WIs e: axial b1000 [c] and [e] ADC. at the same levels detect the same findings with restricted diffusion.

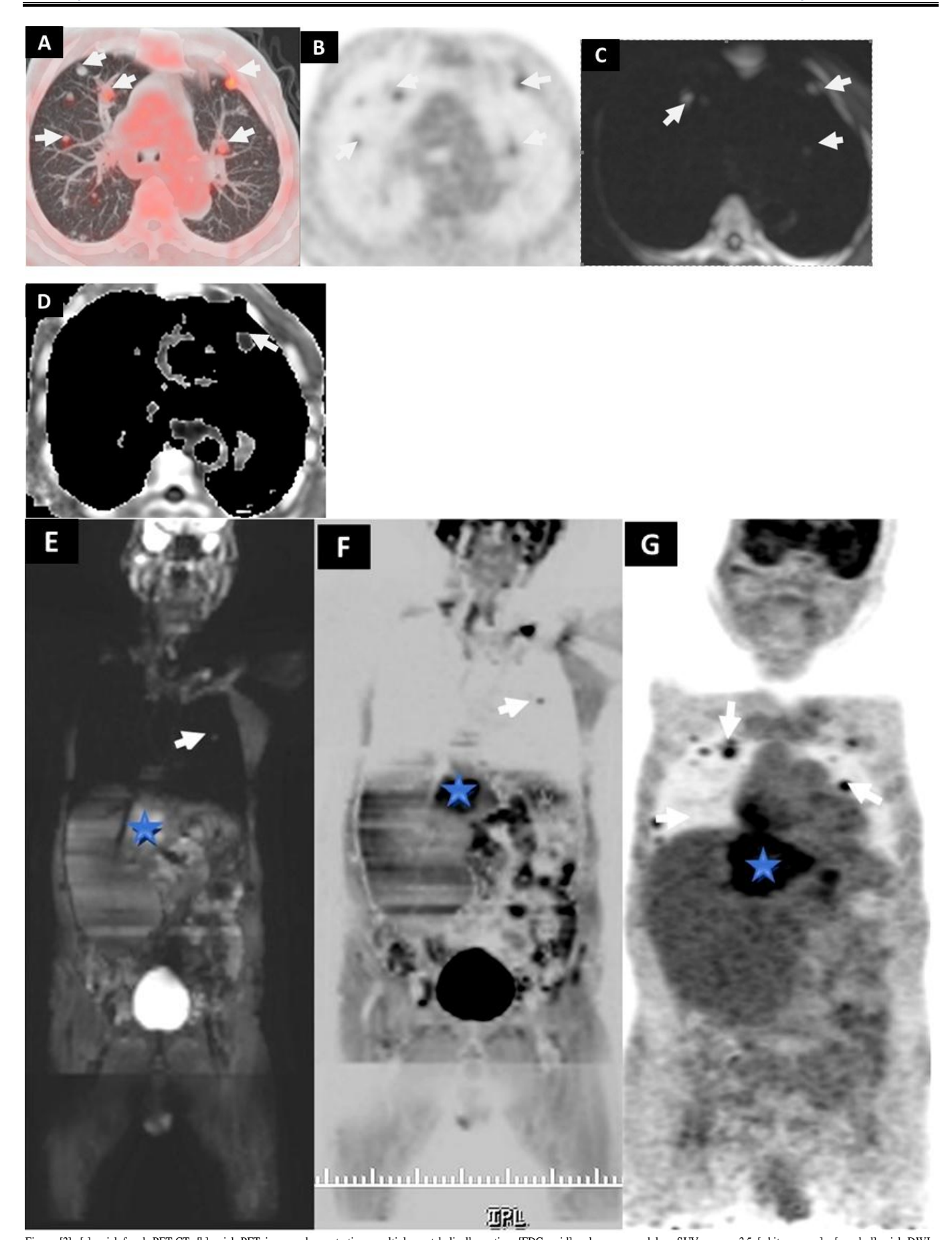


Figure [3]: [a] axial fused PET-CT [b] axial PET images demonstrating multiple metabolically active [FDG axid] pulmonary nodules, SUV max = 3.5 [white arrows]. [c and d] axial DWIs and ADC demonstrating pulmonary nodules showing restricted diffusion [displaying high signal in DWIs and low signal in ADC] but few number compared to PET/CT.[white arrows]. [e, f] coronal DWI positive and negative images and [g] coronal PET Images showing also the pulmonary nodules [white arrow] and ill-defined infiltrative hepatic focal lesion[blue star].

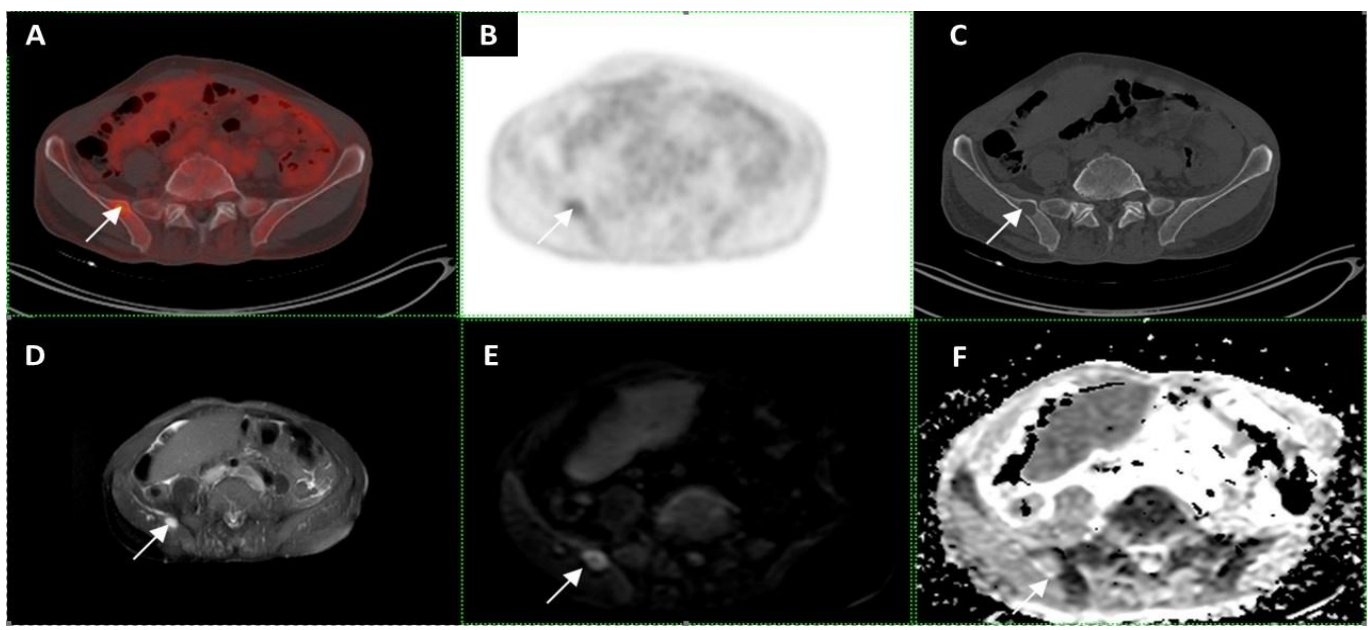


Figure 4: [a]Axial fused PET-CT bone window [b] PET images, [c] axial non contrast CT bone window, versus [d] axial T2 [e, f] Axial DWIS and ADC images for the same case. Both imaging modalities show lytic lesion seen at right iliac bone [white arrows].

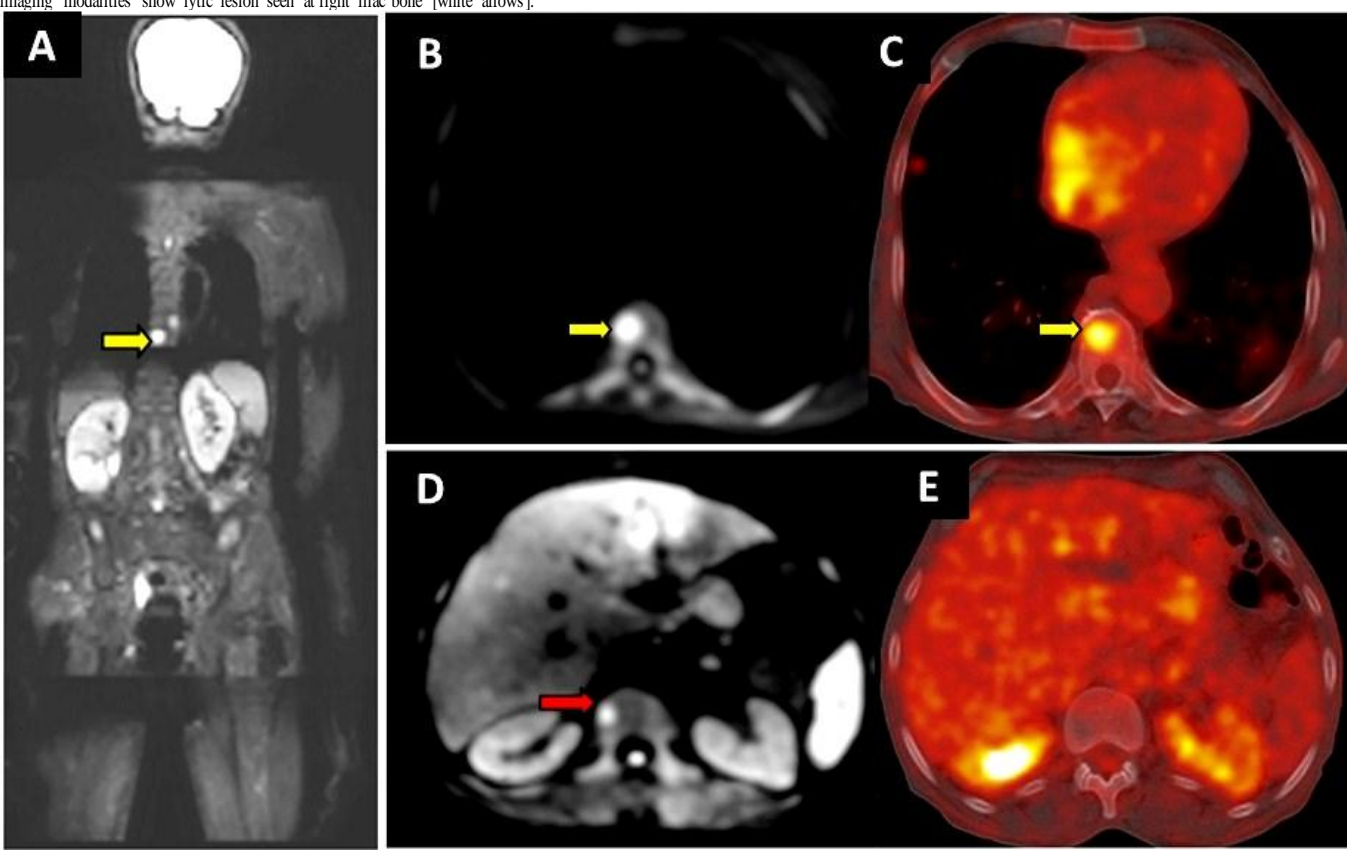


Figure [5]: [a]coronal STAIR, [b] axial DWI and [c] axial fused PET-CT bone window. [a] DV9 vertebral body lesion displaying high signal intensity and diffusion restriction on DWI [b], [c] axial fused PET/CT images bone window demonstrating FDG avid vertebral body lesion at the same level [yellow arrows]. While [d] axial DWI shows a bone lesion at L2 vertebral body with diffusion restriction [red arrow], it is not detected by [e] axial fused PET-CT bone window.

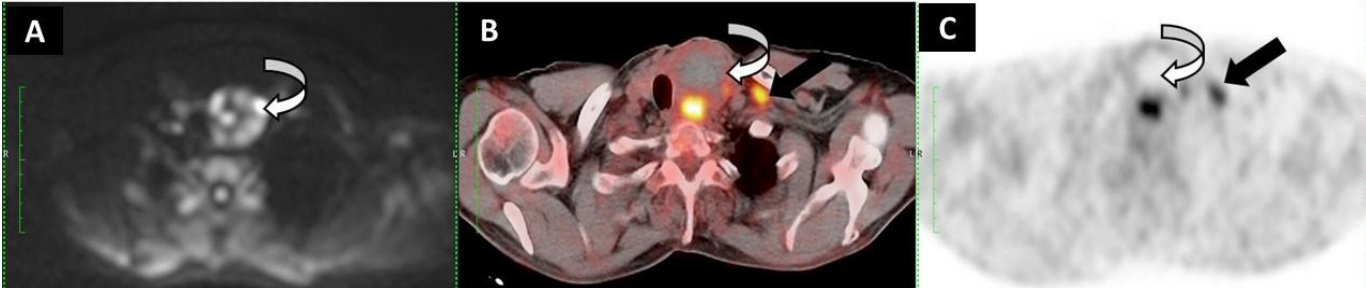


Figure 6: [a, b, c]: [a] axial DWIs [b] axial fused PET/CT and [C] axial PET images. [b and c]: shows left thyroid mass measuring about 5.3x4.5cm with central areas of necrosis and mural calcifications, SUV max 8.3, [previous PET/CT SUV max 3] [curved white arrows], metabolically active enlarged left infraclavicular lymph node with SUV max 5.7 [black arrows]. [a]: left thyroid mass lesion with diffusion restriction, the lymph node not clearly identified.

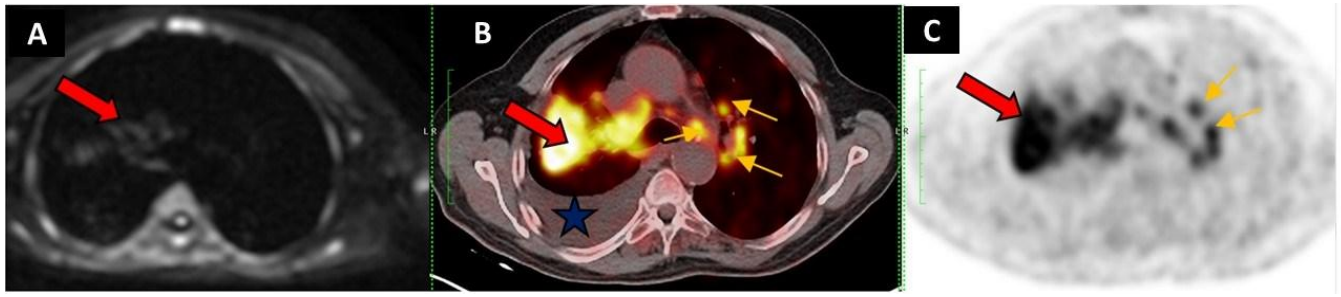


Figure [7]: [a, b, c]: [a] axial DWIs [b] axial fused PET/CT and [C] axial PET images. [b and c]: shows FDG avid right upper lobe soft tissue mass lesion with mediastinal extension, it is seen abutting and compressing right upper bronchus with SUV max 11.5[previous PET/CT SUV max 6.8] [red arrows], metabolically active enlarged mediastinal lymph nodes [yellow arrows], and right sided pleural effusion demonstrating low grade metabolic activity [blue star]. [a]: right upper lobe mass lesion with diffusion restriction [red arrow] but the size is smaller than PET/CT and the lymph node not clearly identified.

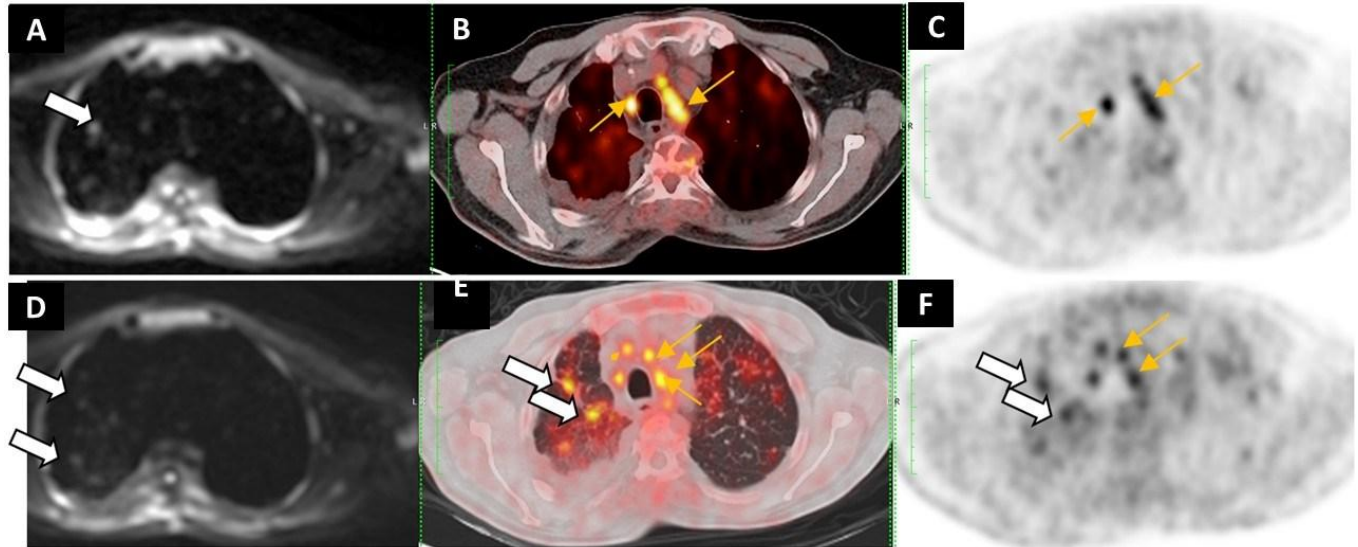


Figure [8]: Axial DWIBS versus Axial PET-CT images for the same case: [a and d] axial b1000 DWI [b&e] axial fused PET-CT and [c and f] PET images. [b, c, e and f] metabolic progression of the mediastinal lymph nodes affecting all groups [yellow arrows], as well as multiple bilateral innumerable pulmonary nodules [white arrows]. [a and d] axial DWI cannot detect the mediastinal lymph nodes, and detect few numbers of pulmonary nodules compared to PET/CT.

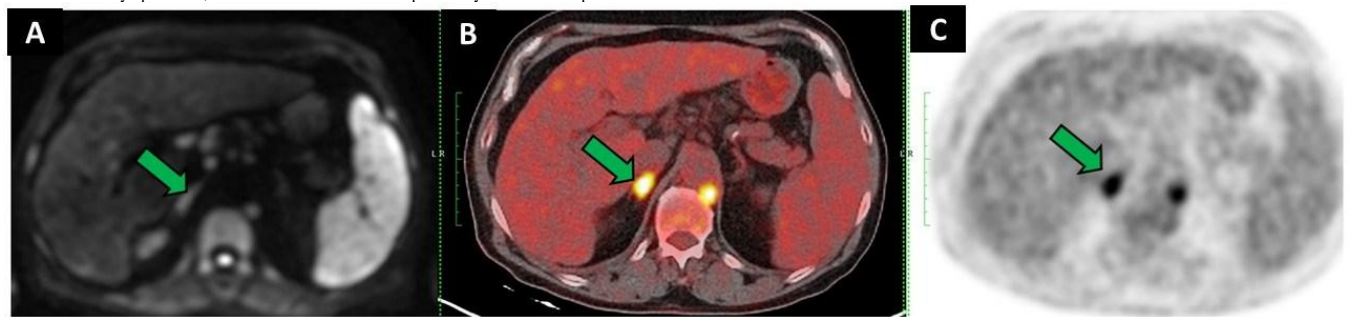


Figure [9]: [a] axial DWIs [b] axial fused PET/CT and [C] axial PET images. [b and c]: shows FDG avid right suprarenal gland lesion with SUV max 11 [green arrows]. [a]: the right suprarenal gland lesion showing diffusion restriction. [green arrow]. So both imaging modalities showing the same finding, They are concordant in detecting adrenal involvement in this case

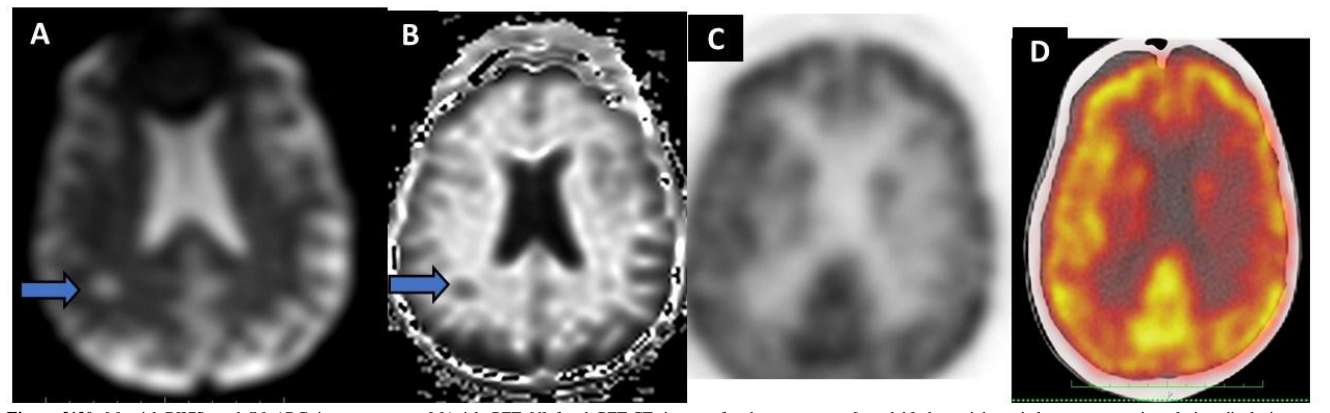


Figure [1]0: [a] axial DWIS and [b] ADC images, versus [c]Axial PET [d] fused PET-CT images for the same case. [a and b] show right parital space occupying lesion displaying restricted diffusion [blue arrows], while the lesion not detected by PET or fused PET/CT images [images c and d]

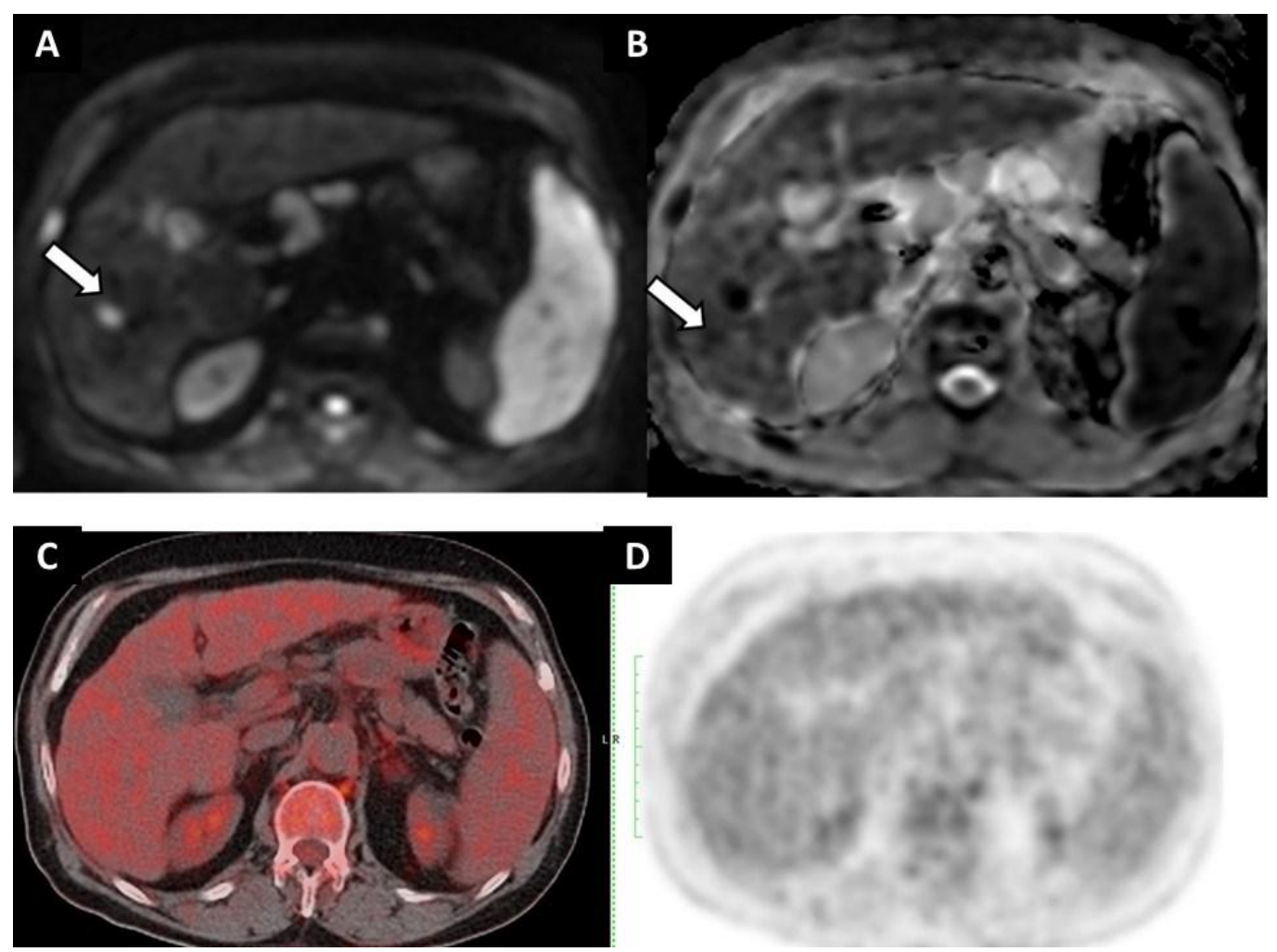


Figure [11]: [a] axial DWIS and [b] ADC images, versus [c]Axial PET [d] fused PET-CT images for the same case. [a and b] show right hepatic lobe segment VI lesion with restricted diffusion [white arrows], while the lesion not detected by PET or fused PET/CT images [images c and d].

### **DISCUSSION**

The present investigation was structured with the primary aim of conducting a comparative analysis between WB-DWI and FDG PET/CT techniques in their ability to detect metastatic lesions originating from a spectrum of primary cancers. A cohort comprising 30 individuals diagnosed with metastases from various initial malignancies participated in this investigation. Each participant underwent both WB-DWI and <sup>18</sup>F-FDG PET/CT scans, scheduled within an average interval of three days, to evaluate the presence of suspected metastatic spread. Furthermore, subtraction imaging proved to be both an efficacious and secure diagnostic approach in identifying hepatocellular carcinoma, particularly following interventions involving Locoregional therapies. For a more streamlined and structured evaluation, the whole-body imaging results were stratified into seven anatomical categories: hepatic structures, pulmonary fields, skeletal framework, lymphatic system, cerebral region, peritoneal cavity, and adrenal glands. The findings revealed a strong concordance between WB-MRI and PET/CT modalities in identifying metastatic involvement in hepatic, osseous, peritoneal, and adrenal regions. In contrast, a moderate level of diagnostic agreement was observed between the two imaging modalities when evaluating pulmonary, lymphatic, and cerebral metastases.

A meticulous and accurate evaluation of the entire body remains a cornerstone in the field of oncology, as it significantly influences diagnostic accuracy, therapeutic strategy formulation, and ongoing monitoring during follow-up [12]. Numerous imaging methodologies

exist for the assessment of malignant diseases; however, the ideal imaging modality is expected to meet several key criteria—it must be broadly accessible, diagnostically accurate, comprehensive in scope, economically viable, time-efficient, and devoid of unnecessary health risks. FDG PET/CT is widely acknowledged as a benchmark imaging modality in the diagnosis of various malignancies. Nevertheless, its utility is hindered in certain healthcare settings due to limited availability, the requisite use of radioactive tracers, and associated radiation exposure [10].

Additional limitations of PET include non-specific tracer uptake in physiologically active tissues, inconsistent tracer retention among different types of lesions, relatively high doses of radiation, and diagnostic ambiguity for nodules measuring less than 1 cm in size [13].

Given these limitations, there is an escalating demand for an imaging approach that not only facilitates a holistic assessment of tumor burden but also enhances lesion detectability and improves diagnostic confidence. Such a modality should ideally support lesion characterization and therapeutic monitoring, all while circumventing the risks associated with ionizing radiation. In response to these diagnostic challenges, recent technological advancements in WB-MRI have made it feasible to perform comprehensive anatomical imaging across the entire body, utilizing T1- and T2-weighted sequences at 1.5T field strength [7]. Key innovations include the implementation of specialized surface coils, continuous table motion systems, refined respiratory gating mechanisms, advanced planning software, and enhanced pulse sequences. These technical developments have collectively propelled

WB-MRI to the forefront, offering robust diagnostic potential in both oncological and non-oncological domains when compared to more traditional imaging techniques <sup>[12]</sup>. To date, MRI applications in oncology have been predominantly anatomical and qualitative in nature. However, there is a growing emphasis on the need to quantify functional tissue parameters accurately, as these measurements may provide early biomarkers indicative of disease progression, even before structural abnormalities become apparent. In particular, advanced MRI techniques—most notably DWI—enable non-invasive evaluation of tumor biology at the molecular level. MRI also presents a significant diagnostic edge over nuclear scintigraphy in detecting marrow infiltration, independent of whether the underlying pathology is osteolytic or osteoblastic in nature <sup>[14]</sup>.

This investigation aimed to assess the diagnostic precision of WB-DWI in identifying metastatic disease and to compare its performance against that of PET/CT, which is widely recognized as a reference imaging modality in oncology. A total of 30 subjects were included, consisting of 16 females [53.3%] and 14 males [46.67%], with a mean age of 52.87 ± 17.07 years [range: 18–74 years]. Breast cancer emerged as the most commonly diagnosed primary malignancy, observed in five female cases. Additionally, five cases [16.67%] were diagnosed with metastatic disease of unknown primary origin. The remaining cases presented with a diverse spectrum of malignancies, including lymphoma; tumors of the female genital tract; testicular and prostatic cancers; and neoplasms arising from the pulmonary and gastrointestinal systems. The diagnostic work-up for the primary tumors involved multiple modalities, including radiological techniques and tissue sampling procedures. Specifically, 11 cases [36.7%] were diagnosed using CT in combination with biopsy. PET/CT was used as the primary diagnostic method in five cases [16.67%]. Another five cases [16.67%] underwent US-guided biopsy, four [13.33%] were diagnosed via CT alone, four [13.33%] were diagnosed by MRI, and one case [3.33%] was identified through BMA. Final confirmation of diagnosis in all cases was achieved through histopathological evaluation.

For clarity and analytic convenience, metastatic sites were classified into seven anatomical regions: liver, lung, skeletal system, LN, peritoneum, brain, and adrenals. Diagnostic accuracy was assessed using a combined reference standard comprising radiologic findings, histopathological confirmation, and approximately six months of clinical follow-up. PET/CT identified 71 metastatic lesions, of which WB-DWI successfully detected 63, reflecting a high level of agreement between both modalities.

In our research the primary tumor diagnosis was by radiological [CT, PET/CT, MRI] and or biopsy, bone marrow aspiration. 11 cases [36.7%] were diagnosed by CT and biopsy, 5 cases [16.67%] were diagnosed by PET/CT, 5 cases [16.67] were diagnosed by US and biopsy, 4 cases [13.33%] were diagnosed by CT, 4 cases [13.33%] were diagnosed by MRI and 1 case [3.33%] was diagnosed by bone marrow aspiration. After which diagnosis was confirmed histo-pathologically.

The metastatic lesions were classified into seven regions for simplifying analysis: liver, lung, skeletal system, lymph nodes, peritoneal, brain, and adrenals metastasis. Using combined radiological and histo-pathologically proven data as well as a follow up about 6 months as a reference standard. Of the 71 metastases detected by PET/CT, 63 were also identified by WB-DWI.

In another research done by **Akdal Dolek and colleagues** [15] employed a more granular regional analysis, wherein metastatic lesions were classified into 18 distinct anatomical regions encompassing the skeletal system, visceral organs, and lymphatic tissues. In that investigation, a total of 378 anatomical regions were scrutinized across 21 cases. Of the 68 metastatic lesions visualized using PET/CT, 64 were

also successfully identified using WB-DWI, thereby reinforcing the diagnostic reliability of WB-DWI as a viable alternative to PET/CT for whole-body metastasis assessment.

### Hepatic metastasis;

In the current research regarding liver metastasis out of the 30 cases were confirmed to have liver metastasis by histopathology and follow up. All the 13 cases were successfully detected by MRI-DWIBS. On the other hand, PET-CT diagnosed 11 out of these 13 cases with 2 false negative instances. Accordingly, the aforementioned data emphasize the significantly higher MRI-DWIBS sensitivity, NPV, and accuracy [P value 0.0012] compared to PET-CT [100% accuracy versus 93.3%], while the similar yield of specificity, PPV was noticed by both techniques [100%]. There is perfect agreement between WB-MRI and PET/CT in detecting liver metastases [WB-MRI can detect all positive 11 cases detected by PET/CT]. perfect [ $\kappa\!=\!0.81$  to  $<\!1.00$ ].

**Dolek and colleagues** <sup>[15]</sup> exhibited that liver metastases were detected in three cases using PET/CT, while WB-DWI identified hepatic lesions in two of these cases. The third lesion, located in segment II of the liver, was not visualized on WB-DWI due to cardiac motion artifacts. Nevertheless, the diagnostic performance of WB-DWI for detecting liver metastases was statistically significant and demonstrated substantial agreement with PET/CT findings [ $\kappa = 0.77$ ; p < .001]. Similarly, **Tahtabasi and colleagues** <sup>[16]</sup> conducted a comparative analysis between MRI and <sup>18</sup>F-FDG PET/CT in the evaluation of hepatic metastases. Their results indicated moderate agreement between the two modalities. Notably, in cases with lesions smaller than 10 mm [n = 10; 23.8%], MRI exhibited superior sensitivity and detected a greater number of metastases than <sup>18</sup>F-FDG PET/CT. This improved detection capability was attributed to MRI's higher spatial resolution, which enhances its ability to identify smaller lesions.

Yang and colleagues [17] conducted a comparative research between gadolinium-enhanced abdominal MRI and <sup>18</sup>F-FDG PET/CT in the detection of hepatic metastases, reporting sensitivities of 85.7% and 71%, respectively. Despite MRI demonstrating higher sensitivity, the difference between the two modalities was not statistically significant. In another research, Yirgin and Koca. <sup>[18]</sup> assessed the effectiveness of whole-body MRI with DWI in detecting liver metastases. They concluded that WB-DWI is a highly practical and reliable tool for evaluating suspected hepatic metastases.

### Pulmonary metastasis: -

In the current research 13 cases were confirmed to have pulmonary metastasis by histopathology and follow-up. All the 13 cases were successfully detected by PET/CT On the other hand, WBDWIs diagnosed 7 out of these 13 cases with 6 false negative instances. Accordingly, the aforementioned data emphasize the significantly higher PET/CT sensitivity, NPV, and accuracy [P value 0.0012] compared to WBDWIs [100% accuracy versus 80%], while the similar yield of specificity, PPV was noticed by both techniques [100%]. There is moderate degree of agreement between WB-MRI and PET/CT in detecting pulmonary metastases [WB-MRI can detect only 7 positive cases from 13 cases detected by PET/CT].

In the research by Akdal Dolek and colleagues [15] <sup>18</sup>F-FDG PET/CT detected lung metastases in six cases, while WB-DWI identified metastases in four of these cases. The agreement between the two modalities was statistically significant and substantial [ $\kappa$  = 0.74; p < .001]. WB-DWI demonstrated a sensitivity of 66.7% and an accuracy of 92.6% for detecting pulmonary metastases. In our own research, WB-DWI exhibited notable limitations in detecting pulmonary lesions smaller than 6 mm. These limitations are attributed to intrinsic challenges in lung imaging with WB-DWI, including low proton

density, susceptibility to respiratory and cardiac motion artifacts, and distortion from air-tissue interfaces. Supporting this, **Regier and colleagues** [33] exhibited sensitivity rates of 86.4% for nodules measuring 6–9 mm and 97% for nodules  $\geq$ 10 mm.

Similarly, **Liu and colleagues** <sup>[19]</sup> conducted a comparative investigation between CT and WB-DWI in the context of evaluating pulmonary metastases originating from renal cell carcinoma. Their findings demonstrated that WB-DWI achieved a sensitivity of 100% in detecting pulmonary nodules exceeding 10mm in diameter. However, its sensitivity markedly decreased to 61.5% for smaller nodules measuring ≤5 mm, highlighting a significant limitation of WB-DWI in detecting subcentimeter pulmonary lesions. Supporting these findings, a meta-analysis <sup>[20]</sup> exhibited pooled diagnostic performance metrics for DWI in the evaluation of malignant pulmonary nodules and masses, yielding an overall sensitivity of 82.8% and specificity of 80.1%.

### **Bony metastasis:**

In our research 15 cases were confirmed to have bone metastasis by histopathology and follow-up. All 15 cases were successfully detected by WBDWIs on the other hand, PET/CT diagnosed 14 out of these 15 cases with 1 false negative instance. Accordingly, the aforementioned data emphasize the significantly higher WBDWIs sensitivity, NPV, and accuracy compared to PET/CT [100% accuracy versus 96.7%], while the similar yield of specificity, PPV was noticed by both techniques [100%]. There is perfect agreement between WB-MRI and PET/CT in detecting bone metastases [WB-MRI can detect all positive 14 cases detected by PET/CT]. perfect [ $\kappa$  = 0.81 to <1.00].

In the research by **Akdal Dolek** *et al.* <sup>[15]</sup> PET/CT scans identified 22 bone metastatic sites, of which 21 [95.4%] were also detected by WB-DWI. The agreement between the two modalities for detecting bone metastases was statistically significant and nearly perfect [ $\kappa$  = 0.90; p < .001], with WB-DWI demonstrating a sensitivity of 85.7% and an accuracy of 96.4%.

Similarly, **Tanaka and colleagues** [21] exhibited that among 80 skeletal metastatic lesions defined by a gold standard, WB-MRI achieved a sensitivity range of 85–93% [p = 0.002–0.21] and a positive predictive value [PPV] of 79–95%. In contrast, <sup>18</sup>F-FDG PET/CT detected 61 lesions, with a sensitivity and PPV of 76% and 75%, respectively. While both modalities performed comparably overall, WB-MRI demonstrated superior sensitivity for skeletal metastasis detection.

Conversely, **Cafagna and colleagues** [22] exhibited differing findings in a retrospective analysis involving various tumor types, concluding that <sup>18</sup>F-FDG PET/CT remained the more effective modality for identifying bone metastases. However, other literature supports the superiority of WB-MRI for this application. WB-MRI has shown enhanced diagnostic performance and interobserver consistency compared to bone scintigraphy and, in many studies, equal or superior accuracy to PET/CT. WB-MRI with DWI offers high diagnostic accuracy for bone metastases due to its sensitivity to changes in bone marrow composition <sup>[23]</sup>.

### Lymph node metastasis: -

In the current research 23 cases were confirmed to have lymph nodal metastasis by histopathology and follow-up. All 23 cases were successfully detected by PET/CT On the other hand, WBDWIs diagnosed 17 out of these 23 cases with 6 false negative instances. Accordingly, the aforementioned data emphasize the significantly higher PET/CT sensitivity, NPV, and accuracy compared to WBDWIs [100% accuracy versus 80%], while the similar yield of specificity, PPV was noticed by both techniques [100%]. There was a moderate degree

of agreement between WB-MRI and PET/CT in detecting lymph nodal metastases [WB-MRI can detect only 17 positive cases from 23 detected by PET/CT]. [moderate [ $\kappa = 0.41$  to 60]].

In the research conducted by Akdal Dolek and colleagues [15] PET/CT imaging of 21 cases identified 31 metastatic lymph node regions. Whole-body diffusion-weighted imaging [WB-DWI] successfully detected all of these lymph node metastases, demonstrating statistically significant diagnostic performance with perfect agreement  $[\kappa = 1; p < .001]$ . Both the sensitivity and accuracy of WB-DWI in detecting lymph node metastases were exhibited at 100%. A recent meta-analysis examining metastatic mediastinal lymph nodes in nonsmall cell lung cancer [NSCLC] exhibited that both 18F-FDG PET/CT and DWI exhibited high specificity but relatively low sensitivity [24]. Komori and colleagues [25] compared 18F-FDG PET/CT and diffusionweighted whole-body imaging with background body signal suppression [DWIBS], analyzing both image quality and quantitative measures. Their results indicated that ADC values alone were insufficient for reliably differentiating malignant from benign lesions. Stecco and colleagues [26] in a pilot research involving oncologic cases with various tumor types, assessed MR-DWIBS against <sup>18</sup>F-FDG PET/CT and exhibited that MR-DWIBS exhibited high sensitivity and specificity in staging. Similarly, Sui and colleagues [27] demonstrated that DWI achieved sensitivities and specificities of 72% and 96% for thoracic lymph node metastasis, and 82% and 90% for abdominal lymph node metastasis, respectively.

### Brain metastasis: -

In the current research 6 out of the 30 cases were confirmed to have brain metastasis by histopathology and follow up. Five cases out of these 6 were successfully detected by MRI-DWIBS with 1 false negative case. On the other hand, PET-CT diagnosed 3 out of these 6 cases with 3 false negative instances. Accordingly, the aforementioned data emphasize the significantly higher MRI-DWIBS sensitivity, NPV, and accuracy compared to PET-CT [96.7% accuracy versus 90.0%], while the similar yield of specificity, PPV was noticed by both techniques [100%]. There was a moderate degree of agreement between WB-MRI and PET/CT in detecting brain metastases [WB-MRI can detect 2 positive cases from 3 cases detected by PET/CT] moderate [ $\kappa = 0.41$ -0.60].

In a prospective analysis, the diagnostic capabilities of FDG-PET/CT and WB-MRI were systematically compared for TNM staging in 165 cases with NSCLC. The results highlighted a complementary diagnostic profile: WB-MRI exhibited superior sensitivity for detecting cerebral and hepatic metastases, whereas FDG-PET/CT was more effective for identifying lymphatic and soft-tissue involvement. Despite these modality-specific strengths, both approaches demonstrated equivalent overall accuracy in metastasis detection [86%].

Similarly, **Chen and colleagues** <sup>[28]</sup> compared WB-DWI and FDG-PET/CT in NSCLC diagnosis and confirmed that WB-MRI had an advantage in detecting brain and liver metastases, while PET/CT remained more sensitive for nodal and soft-tissue lesions.

### Suprarenal metastasis: -

The findings of our investigation demonstrated that both PET/CT and MRI-DWIBS exhibited exceptional diagnostic performance in the detection of adrenal metastases, achieving 100% sensitivity, specificity, PPV, NPV, and overall diagnostic accuracy for this site. Notably, there was a high level of concordance between WB-MRI and PET/CT in identifying adrenal involvement, with WB-MRI successfully detecting all three adrenal metastases identified by PET/CT. This diagnostic agreement was classified as *perfect*, based on a  $\kappa$  coefficient ranging from 0.81 to <1.00, indicating strong statistical consistency between the two modalities. These results are consistent with prior research by Akdal

**Dolek and colleagues** <sup>[15]</sup>, in which WB-DWI successfully detected all instances of adrenal and soft tissue metastases. Their analysis exhibited a  $\kappa$  value of 1, signifying perfect agreement, with the association reaching strong statistical significance [p < .001]. These findings reinforce the reliability of WB-DWI as a highly accurate and non-invasive modality for the detection of adrenal metastatic disease, similar to the performance of PET/CT in this anatomical region.

### Peritoneal metastasis:

Regarding to peritoneal metastasis there are 4 cases were confirmed to have peritoneal metastasis by histopathology and follow-up. All 4 cases were successfully detected by PET/CT On the other hand, WBDWIs diagnosed 3 out of these 4 cases with 1 false negative instance. Accordingly, the aforementioned data emphasize the significantly higher PET/CT sensitivity, NPV, and accuracy compared to WBDWIs [100% accuracy versus 96.7%], while the similar yield of specificity, PPV was noticed by both techniques [100%]. There is a good degree of agreement between WB-MRI and PET/CT in detecting peritoneal metastases [WB-MRI can detect only 3 positive cases from 4 detected by PET/CT] perfect [ $\kappa\!=\!0.81$  to  $<\!1.00$ ].

In a comparative evaluation conducted by **Schmidt** *et al.* <sup>[29]</sup> the diagnostic performances of CT, MRI, and PET/CT were assessed in the context of detecting peritoneal carcinomatosis. The investigation exhibited sensitivities of 96% for CT, 98% for MRI, and 95% for PET/CT, alongside specificities of 92%, 84%, and 96%, respectively. While MRI demonstrated the highest sensitivity among the three modalities—suggesting superior capability in identifying true-positive cases—PET/CT achieved the highest specificity, reflecting its strength in accurately ruling out non-malignant conditions. Despite these variations in diagnostic metrics, the investigation concluded that the differences in performance among CT, MRI, and PET/CT were not statistically significant.

van't Sant and colleagues [30] conducted a meta-analysis that demonstrated DW-MRI as having the highest sensitivity for detecting peritoneal metastases in cases with gastrointestinal or ovarian cancers. In comparison, PET/CT exhibited slightly lower diagnostic performance, although the difference was not statistically significant. Specifically, the pooled sensitivity and specificity for PET/CT were 80% [CI, 57–92%] and 90% [CI, 80–96%], respectively, while for DW-MRI, these values were 92% [CI, 84–96%] and 85% [CI, 78–91%]. Despite this, DW-MRI offers greater accessibility in clinical practice than PET/CT, positioning it as a potential imaging modality of choice. In contrast, CT demonstrated the lowest sensitivity among the modalities, with a sensitivity of 68% [CI, 46–84%].

While WB-DWI presents several advantages, including its ability to detect metastases without ionizing radiation and its high sensitivity in certain regions, it also has notable limitations. One key issue is its susceptibility to artifacts. The technique can be affected by motion artifacts, particularly in regions with high air content [such as the lungs], as well as cardiac and respiratory motion, which can lead to reduced image quality and diagnostic accuracy [30].

Furthermore, lower spatial resolution compared to PET/CT can make it challenging to detect smaller lesions, particularly those less than 1 cm, which can be a significant drawback in detecting early-stage metastatic disease [31]. In our study, WB-DWI showed limitations in detecting smaller pulmonary lesions [less than 6 mm], which aligns with findings in the literature indicating that WB-DWI's sensitivity for smaller nodules is lower compared to PET/CT [32,33].

Another limitation of WB-DWI is the longer scan times required for whole-body imaging, which can lead to patient discomfort and reduced compliance, especially in critically ill or elderly patients. Additionally, the lack of contrast agents in WB-DWI means that it may struggle to differentiate between benign and malignant lesions in certain organ systems, especially when lesions have similar signal characteristics [34].

Despite these limitations, WB-DWI has shown promise as a valuable tool in the detection of metastatic disease. Recent advancements, such as improved pulse sequences and motion correction techniques, are expected to address some of these issues, and ongoing research will continue to refine the utility of WB-DWI in clinical practice [35].

In conclusion, WB-DWI proves to be a highly effective tool for detecting both visceral and bone metastatic lesions in cases with solid tumors, offering diagnostic accuracy similar to that of PET/CT. Metastatic lesions consistently exhibit lower ADC values when compared to normal healthy tissue. There is a moderate to good level of agreement between WB-DWI and PET/CT for metastasis screening, with the combined use of both modalities enhancing the detection accuracy and revealing additional lesions beyond those identified through conventional imaging alone. Further research with larger case cohorts is necessary to validate the promising results observed in this research.

Additionally, the role of quantitative ADC analysis in improving WB-DWI performance warrants further investigation, particularly through the use of multiple b-values to refine the accuracy of ADC measurements. We recommend incorporating WB-DWI into routine metastatic work-up protocols, as its combination with conventional imaging significantly improves the detection rate of metastatic lesions, thus potentially expanding the scope of clinical evaluation.

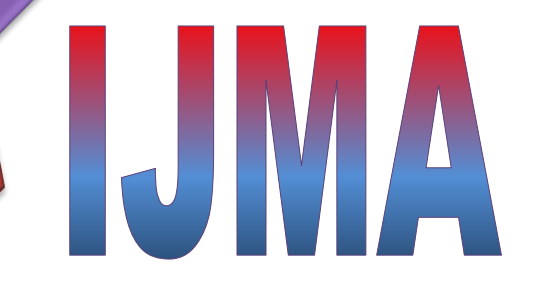
Financial and non-financial activities and relationships of interest: None.

### REFERENCES

- Das S, Dey MK, Devireddy R, Gartia MR. Biomarkers in Cancer Detection, Diagnosis, and Prognosis. Sensors [Basel]. 2023 Dec 20; 24[1]:37. doi: 10.3390/s24010037.
- Bailey S, Hackney D, Vashishth D, Alkalay RN. The effects of metastatic lesion on the structural determinants of bone: Current clinical and experimental approaches. Bone. 2020 Sep; 138:115159. doi: 10.1016/j.bone.2019.115159.
- Haldorsen IS, Lura N, Blaakær J, Fischerova D, Werner HMJ. What Is the Role of Imaging at Primary Diagnostic Work-Up in Uterine Cervical Cancer? Curr Oncol Rep. 2019 Jul 29; 21[9]:77. doi: 10.1007/s11912-019-0824-0.
- Hassan HA, El Sheikh HES, Abdelmonem AA. Role of Whole Body Diffusion Magnetic Resonant Imaging in detection of metastatic disease. Benha Med J. 2022; 39[2]:472-81. doi: 10.21608/bmfj.2022.18321.1104.
- Zytoon AA, Elsayed EE, Nassar AI, Murakami K. Pivotal role of PET/CT in characterization of occult metastasis with undetermined origin. Egypt J Radiol Nucl Med. 2020; 51[4]:1-11. doi: 10.1186/s43055-020-00357-1
- 6. Trotter J, Pantel AR, Teo BK, Escorcia FE, Li T, Pryma DA, Taunk NK. Positron Emission Tomography [PET]/Computed Tomography [CT] Imaging in Radiation Therapy Treatment Planning: A Review of PET Imaging Tracers and Methods to Incorporate PET/CT. Adv Radiat Oncol. 2023 Mar 27;8[5]:101212. doi: 10.1016/j.adro.2023.101212.
- Jacobs MA, Macura KJ, Zaheer A, Antonarakis ES, Stearns V, Wolff AC, et al. Multiparametric Whole-body MRI with Diffusion-weighted Imaging and ADC Mapping for the Identification of Visceral and Osseous Metastases From Solid Tumors. Acad Radiol. 2018 Nov;25[11]:1405-1414. doi: 10.1016/j.acra.2018.02.010.

- Baliyan V, Das CJ, Sharma R, Gupta AK. Diffusion weighted imaging: Technique and applications. World J Radiol. 2016 Sep 28;8[9]:785-798. doi: 10.4329/wjr.v8.i9.785.
- Horvat JV, Bernard-Davila B, Helbich TH, Zhang M, Morris EA, Thakur SB, et al. Diffusion-weighted imaging [DWI] with apparent diffusion coefficient [ADC] mapping as a quantitative imaging biomarker for prediction of immunohistochemical receptor status, proliferation rate, and molecular subtypes of breast cancer. J Magn Reson Imaging. 2019 Sep;50[3]:836-846. doi: 10.1002/jmri.26697.
- Paruthikunnan SM, Kadavigere R, Karegowda LH. Accuracy of Whole-Body DWI for Metastases Screening in a Diverse Group of Malignancies: Comparison With Conventional Cross-Sectional Imaging and Nuclear Scintigraphy. AJR Am J Roentgenol. 2017 Sep;209[3]:477-490. doi: 10.2214/AJR.17.17829.
- Barchetti F, Stagnitti A, Megna V, Al Ansari N, Marini A, Musio D, et al. Unenhanced whole-body MRI versus PET-CT for the detection of prostate cancer metastases after primary treatment. Eur Rev Med Pharmacol Sci. 2016 Sep; 20[18]:3770-3776. PMID: 27735042.
- Axelsen MB, Eshed I, Østergaard M, Hetland ML, Møller JM, Jensen DV, et al. Monitoring total-body inflammation and damage in joints and entheses: the first follow-up study of whole-body magnetic resonance imaging in rheumatoid arthritis. Scand J Rheumatol. 2017 Jul;46[4]:253-262. doi: 10.1080/03009742.2016.1231338.
- Yang HL, Liu T, Wang XM, Xu Y, Deng SM. Diagnosis of bone metastases: a meta-analysis comparing <sup>18</sup>FDG PET, CT, MRI and bone scintigraphy. Eur Radiol. 2011 Dec;21[12]:2604-17. doi: 10.1007/s00330-011-2221-4.
- Ei Khouli RH, Jacobs MA, Mezban SD, Huang P, Kamel IR, Macura KJ, Bluemke DA. Diffusion-weighted imaging improves the diagnostic accuracy of conventional 3.0-T breast MR imaging. Radiology. 2010 Jul;256[1]:64-73. doi: 10.1148/radiol.10091367.
- Akdal Dolek B, Sozmen Ciliz D, Ozdemir N, Ozet G, Duran S. Comparative Analysis of Whole-Body Diffusion-Weighted Imaging and PET/CT in Metastasis Detection: A Prospective Study. Cureus. 2024 Nov 29;16[11]:e74756. doi: 10.7759/cureus.74756.
- Tahtabasi M, Erturk SM, Basak M. Comparison of MRI and 18F-FDG PET/CT in the Liver Metastases of Gastrointestinal and Pancreaticobiliary Tumors. Sisli Etfal Hastan Tip Bul. 2021 Mar 17; 55[1]:12-17. doi: 10.14744/SEMB.2020.80270.
- Yang M, Martin DR, Karabulut N, Frick MP. Comparison of MR and PET imaging for the evaluation of liver metastases. J Magn Reson Imaging. 2003 Mar;17[3]:343-9. doi: 10.1002/jmri.10265.
- Yirgin I, Koca D. Diffusion-weighted magnetic resonance imaging [DW-MRI] in suspected liver metastasis. Int J Radiol Radiat Ther. 2019; 6[1]:11-5. Available at: <a href="https://medcraveonline.com/">https://medcraveonline.com/</a> <a href="https://medcraveonline.com/">JJRRT/JJRRT-06-00204.pdf</a>, Last accessed, June 2025.
- Liu J, Yang X, Li F, Wang X, Jiang X. Preliminary study of whole-body diffusion-weighted imaging in detecting pulmonary metastatic lesions from clear cell renal cell carcinoma: comparison with CT. Acta Radiol. 2011 Nov 1;52[9]:954-63. doi: 10.1258/ar.2011.110121.
- Li B, Li Q, Chen C, Guan Y, Liu S. A systematic review and meta-analysis
  of the accuracy of diffusion-weighted MRI in the detection of malignant
  pulmonary nodules and masses. Acad Radiol. 2014 Jan;21[1]:21-9. doi:
  10.1016/j.acra.2013.09.019.
- Tanaka Y, Nakanishi K, Ueda T, Nakazawa T, Oshima K. Retrospective comparative study between 3T WB-MRI including WB-DWI and 18F-FDG-PET/CT in detection of metastatic disease. Cancer Reports and Reviews 2017;1[6]:1-5. doi: 10.15761/CRR.1000135.
- Cafagna D, Rubini G, Iuele F, Maggialetti N, Notaristefano A, Pinto D, et al. Whole-body MR-DWIBS vs. [18F]-FDG-PET/CT in the study of malignant tumors: a retrospective study. Radiol Med. 2012 Mar;117[2]:293-311. doi: 10.1007/s11547-011-0708-3.

- Pearce T, Philip S, Brown J, Koh DM, Burn PR. Bone metastases from prostate, breast and multiple myeloma: differences in lesion conspicuity at short-tau inversion recovery and diffusion-weighted MRI. Br J Radiol. 2012 Aug;85[1016]:1102-6. doi: 10.1259/bjr/30649204.
- Shen G, Hu S, Deng H, Kuang A. Performance of DWI in the Nodal Characterization and Assessment of Lung Cancer: A Meta-Analysis. AJR Am J Roentgenol. 2016 Feb;206[2]:283-90. doi: 10.2214/AJR.15.15032.
- Komori T, Narabayashi I, Matsumura K, Matsuki M, Akagi H, Ogura Y, Aga F, Adachi I. 2-[Fluorine-18]-fluoro-2-deoxy-D-glucose positron emission tomography/computed tomography versus whole-body diffusion-weighted MRI for detection of malignant lesions: initial experience. Ann Nucl Med. 2007 Jun;21[4]:209-15. doi: 10.1007/s12149-007-0010-6.
- Stecco A, Romano G, Negru M, Volpe D, Saponaro A, Costantino S, et al. Whole-body diffusion-weighted magnetic resonance imaging in the staging of oncological patients: comparison with positron emission tomography computed tomography [PET-CT] in a pilot study. Radiol Med. 2009 Feb;114[1]:1-17. English, Italian. doi: 10.1007/s11547-008-0348-4.
- Sui WF, Chen X, Peng ZK. Applying diffusion-weighted imaging to detect metastatic and non-metastatic lymph nodes in abdomen: a meta-analysis and systematic review. Applied Magnetic Resonance 2016.47[4]:951-63; doi:10.1007/s00723-016-0808-2.
- Chen W, Jian W, Li HT, Li C, Zhang YK, Xie B, et al. Whole-body diffusion-weighted imaging vs. FDG-PET for the detection of non-smallcell lung cancer. How do they measure up? Magn Reson Imaging. 2010 Jun;28[5]:613-20. doi: 10.1016/j.mri.2010.02.009.
- Schmidt GP, Reiser MF, Baur-Melnyk A. Whole-body imaging of the musculoskeletal system: the value of MR imaging. Skeletal Radiol. 2007 Dec;36[12]:1109-19. doi: 10.1007/s00256-007-0323-5.
- Albano D, La Grutta L, Grassedonio E, Patti C, Lagalla R, Midiri M, Galia M. Pitfalls in whole body MRI with diffusion weighted imaging performed on patients with lymphoma: What radiologists should know. Magn Reson Imaging. 2016 Sep;34[7]:922-31. doi: 10.1016/j.mri.2016.04.023.
- Akdal Dolek B, Sozmen Ciliz D, Ozdemir N, Ozet G, Duran S. Comparative Analysis of Whole-Body Diffusion-Weighted Imaging and PET/CT in Metastasis Detection: A Prospective Study. Cureus. 2024 Nov 29;16[11]:e74756. doi: 10.7759/ cureus.74756.
- 32. Lother D, Robert M, Elwood E, Smith S, Tunariu N, Johnston SRD, et al. Imaging in metastatic breast cancer, CT, PET/CT, MRI, WB-DWI, CCA: review and new perspectives. Cancer Imaging. 2023 May 31; 23[1]:53. doi: 10.1186/s40644-023-00557-8.
- 33. Regier M, Schwarz D, Henes FO, Groth M, Kooijman H, Begemann PG, Adam G. Diffusion-weighted MR-imaging for the detection of pulmonary nodules at 1.5 Tesla: intraindividual comparison with multidetector computed tomography. J Med Imaging Radiat Oncol. 2011 Jun;55[3]:266-74. doi: 10.1111/j.1754-9485.2011.02263.x..
- Michielsen KL, Vergote I, Dresen R, Op de Beeck K, Vanslembrouck R, Amant F, et al. Whole-body diffusion-weighted magnetic resonance imaging in the diagnosis of recurrent ovarian cancer: a clinical feasibility study. Br J Radiol. 2016 Nov;89[1067]:20160468. doi: 10.1259/bjr.20160468.
- Partridge SC, Nissan N, Rahbar H, Kitsch AE, Sigmund EE. Diffusion-weighted breast MRI: Clinical applications and emerging techniques. J Magn Reson Imaging. 2017 Feb;45 [2]:337-355. doi: 10.1002/jmri.25479.





# INTERNATIONAL JOURNAL OF MEDICAL

ARTS

Volume 7, Issue 8 (August 2025)



http://ijma.journals.ekb.eg/

P-ISSN: 2636-4174

E-ISSN: 2682-3780